

All-optical control of photon statistics with hybrid quantum plasmonic system

Dongxing Zhao¹

¹*School of Physical Science and Technology, Southwest University, Chongqing 400715, China*

(Dated: December 14, 2024)

We propose an all-optical scheme to control the photon statistics using hybrid quantum plasmonic system. With the aid of dressed states, it is shown that the photon correlation of signal field can be continuously modulated from bunching to antibunching under the control of a pump field. Apart from the exact multimode model, we identify the roles of multimode coupling and quantum interference between probability amplitudes, peculiar to the studied system, through a single-mode model and an analytical treatment. Different from the cavity quantum electrodynamics methods, the proposed scheme works well in the bad cavity limit. These findings suggested that this hybrid system provides a feasible nanophotonic platform for active modulation of photon correlation and for future quantum devices.

Due to excellent abilities to engineer the field-matter interaction, the hybrid quantum plasmonic system opens an alternative possibility to the realization of quantum-controlled devices [1]. Among the rich variety of hybrid quantum plasmonic system, the assembly of quantum emitter (QE) and metallic nanoparticle (MNP) plays a prominent role in the realization of coherent coupling between single photons and emitters on the nanoscale. To explore its potential application in the quantum science, various quantum optical properties of the hybrid QE-MNP system have been studied theoretically on the one hand, such as strong coupling [2–6], photon statistics [7–11], squeezing [12, 13] and entanglement [14–20]. On the other hand, remarkable experimental progresses about the Fano resonance [21–23] and strong coupling [24, 25] of the QE-MNP system were reported. Though these rapid progresses promise the realization of more complex nanoscaled quantum devices, the dependence of fabrication process or choice of dielectric environment to tune its optical response raises certain difficulties for practical application. Thus it is highly desirable to develop the active way to control the quantum optical properties of QE-MNP system.

Characterized by equal-time second-order correlation function $g^{(2)}(0)$, the photon statistics exhibits the non-classical features of light [26]. A value of $g^{(2)}(0) < 1$ (> 1) demonstrates the antibunching (bunching) statistics. The generation of nonclassical light fields, for instance the antibunched light, is key to quantum networks [27] as well as quantum-optical spectroscopy [28]. The traditional ways to tune the photon statistics generally rely on the cavity quantum electrodynamics (CQED) system which consists of QEs and optical microcavities. For instance, both antibunched and bunched light can be obtained with the methods based on photon blockade and photon-induced tunneling effects [29, 30], cavity electromagnetically induced transparency [31, 32], or nonlinearity of coupled cavities [33, 34]. However, the dependence of strong coupling and micrometer size of CQED system raise certain difficulties for its ultracompact integration and practical application. Therefore, it is preferable to tune the photon statistics with a more feasible and compact scheme.

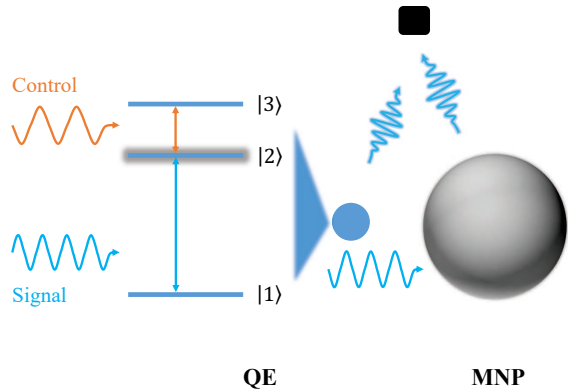


FIG. 1. Schematic of the hybrid system composed of a QE and a spherical MNP. Both the dipole mode of MNP and QE transition $|1\rangle \leftrightarrow |2\rangle$ are driven by the signal field. In addition, the QE transition $|1\rangle \leftrightarrow |2\rangle$ couples to all the plasmon modes of MNP. A control field which drives the transition $|2\rangle \leftrightarrow |3\rangle$ is also introduced.

Here we investigate the all-optical modulation of photon correlation with the hybrid QE-MNP system. The photon statistics can be tuned from bunching to antibunching with a control field. Different from the CQED system, the QE-MNP system can control the photon statistics without the need of strong coupling condition. To characterise the quantum nature of the studied system and perform in-depth study on this control scheme, we provide exact multimode quantum model which works beyond the dipole approximation. In addition, an approximate single-mode model and analytical expressions are also derived. It is found that enriched by the dressed states, the quantum interferences between the probability amplitudes play a vital role in the modulation of photon statistics.

Exact multimode model.—We consider a hybrid quantum plasmonic system comprised of a ladder-type three-level QE and spherical MNP with radius r_m and dielectric constant ϵ_m , as shown in Fig. 1. The QE and MNP are separated by distance R and embedded in a dielectric host (permittivity ϵ_b). MNP is able to support localized

surface plasmon resonance, with the resonance frequency ω_n determined by $\text{Re}[\varepsilon_m(\omega_n)] = -\frac{n+1}{n}\varepsilon_b$ ($n = 1, 2, 3, \dots$) for spherical MNP whose radius is much smaller than the plasmon wavelength [35]. Contrast to the dipole mode ($n = 1$), the higher modes ($n \geq 2$) cannot couple to an plane wave because of their vanishing dipole moment. The QE transition $|1\rangle \leftrightarrow |2\rangle$ (frequency ω_{21} , decay rate γ_{21} , transition dipole moment μ) is coupled by all the MNP modes as well as a weak signal field, with frequency ω_s and Rabi frequency $\Omega_{s\mu}$, while the transition $|2\rangle \leftrightarrow |3\rangle$ (frequency ω_{32} , decay rate γ_{32}) is only coupled by a control field, with frequency ω_c and Rabi frequency Ω_c . In addition, the dipole mode of MNP (dipole moment χ) is also driven by the signal field, with Rabi frequency $\Omega_{s\chi}$. The Hamiltonian of the hybrid system in a rotating frame within the rotating-wave approximation reads ($\hbar = 1$)

$$H = \Delta_s \sigma_{22} + (\Delta_s + \Delta_c) \sigma_{33} + \sum_{n=1}^N \Delta_n a_n^\dagger a_n - \sum_{n=1}^N g_n (a_n \sigma_{21} + \text{H.c.}) - (\Omega_{s\mu} \sigma_{12} + \Omega_c \sigma_{23} + \Omega_{s\chi} a_1 + \text{H.c.}), \quad (1)$$

where a_n (a_n^\dagger) is the annihilation (creation) operator of the n th mode of MNP, σ_{ij} ($i, j = 1, 2, 3$) stands for a population operator for $i = j$ and a dipole transition operator for $i \neq j$, and H.c. represents Hermitian conjugate. The detunings are defined by $\Delta_s = \omega_{21} - \omega_s$, $\Delta_c = \omega_{32} - \omega_c$, and $\Delta_n = \omega_n - \omega_s$. The first three terms in Eq. (1) are the free Hamiltonian of the hybrid system. Note that N modes have been taken into consideration at most, which should be determined by the convergence of steady state results. The remaining terms describe the coupling between n th mode of MNP and QE transition $|1\rangle \leftrightarrow |2\rangle$, with coupling constants g_n determined by $g_n = \frac{\mu}{R^{n+2}} \sqrt{\frac{2n+1}{n} \frac{s_n \eta_n r_m^{2n+1}}{4\pi\hbar\varepsilon_0}}$, where $\eta_n = 1/\frac{d}{d\omega} \text{Re}[\varepsilon_m(\omega)]|_{\omega=\omega_n}$ and $s_n = (n+1)^2 (n(n+1)/2)$ for a radial (tangential) QE [9]. The last terms describe the coupling between the hybrid system and external fields. As both the transition $|1\rangle \leftrightarrow |2\rangle$ and dipole mode of MNP are driven by the signal field, the ratio ξ of $\Omega_{s\chi}$ and $\Omega_{s\mu}$ can be simply given by the ratio of χ and μ , i.e. $\xi = \Omega_{s\chi}/\Omega_{s\mu} = \chi/\mu = \varepsilon_b \sqrt{12\pi\hbar\varepsilon_0\eta_1 r_m^3}/\mu$ [9].

The full dynamics of the system is governed by the master equation

$$\dot{\rho} = i[\rho, H] + \frac{\gamma_{21}}{2} (2\sigma_{12}\rho\sigma_{21} - \sigma_{22}\rho - \rho\sigma_{22}) + \frac{\gamma_{32}}{2} (2\sigma_{23}\rho\sigma_{32} - \sigma_{33}\rho - \rho\sigma_{33}) + \sum_{n=1}^N \frac{\kappa_n}{2} (2a_n \rho a_n^\dagger - a_n^\dagger a_n \rho - \rho a_n^\dagger a_n), \quad (2)$$

with $\kappa_n = 2\eta_n \text{Im}[\varepsilon_m(\omega_n)]$ being the decay rate of n th mode of the MNP. Under the conditions of weak pumping and small N , this equation can be numerically solved using the open-source software QuTiP [36, 37].

Effective single-mode model.—Though above multimode model gives the exact description of the studied system, the calculations become unfeasible as the QE close to MNP, which may lead to exceedingly large dimension of density matrix. In order to solve this problem and identify the role of higher-modes, we derive an equivalent effective Hamiltonian

$$H_{\text{eff}} = \Delta_{s,\text{eff}} \sigma_{22} + (\Delta_{s,\text{eff}} + \Delta_{c,\text{eff}}) \sigma_{33} + \Delta_1 a_1^\dagger a_1 - g_1 (a_1 \sigma_{21} + \text{H.c.}) - (\Omega_{s\mu} \sigma_{12} + \Omega_c \sigma_{23} + \Omega_{s\chi} a_1 + \text{H.c.}), \quad (3)$$

and the corresponding effective master equation

$$\dot{\rho}_{\text{eff}} = i[\rho_{\text{eff}}, H_{\text{eff}}] + \frac{\gamma_{21,\text{eff}}}{2} (2\sigma_{12}\rho_{\text{eff}}\sigma_{21} - \sigma_{22}\rho_{\text{eff}} - \rho_{\text{eff}}\sigma_{22}) + \frac{\gamma_{32}}{2} (2\sigma_{23}\rho_{\text{eff}}\sigma_{32} - \sigma_{33}\rho_{\text{eff}} - \rho_{\text{eff}}\sigma_{33}) + \frac{\kappa_1}{2} (2a_1 \rho_{\text{eff}} a_1^\dagger - a_1^\dagger a_1 \rho_{\text{eff}} - \rho_{\text{eff}} a_1^\dagger a_1), \quad (4)$$

where the effective detunings $\Delta_{s,\text{eff}}$, $\Delta_{c,\text{eff}}$, and decay rates $\gamma_{21,\text{eff}}$ are derived as

$$\begin{aligned} \Delta_{s,\text{eff}} &= \Delta_s - \sum_{n=2}^N \alpha_n (\omega_n - \omega_x), \\ \Delta_{c,\text{eff}} &= \Delta_c + \sum_{n=2}^N \alpha_n (\omega_n - \omega_x), \\ \gamma_{21,\text{eff}} &= \gamma_{21} + \sum_{n=2}^N \alpha_n (\gamma_n - \gamma_x), \end{aligned} \quad (5)$$

with $\alpha_n = \frac{g_n^2}{(\omega_n - \omega_{21})^2 + (\kappa_n - \gamma_{21})^2/4}$. This effective model is derived with adiabatic elimination method, under the condition of $\alpha_n \ll 1$. For the realistic parameter, this approximation is valid as long as the QE is not in close proximity to MNP. This model not only greatly simplifies the calculation process, but also reveals that the roles of MNP higher-modes are to shift and broaden the level $|2\rangle$ of QE. To be more specific, the transition frequency between QE level $|1\rangle$ and $|2\rangle$ is modified to be $\omega_{21,\text{eff}} = \omega_{21} - \sum_{n=2}^N \alpha_n (\omega_n - \omega_{21})$ by higher modes of MNP.

Control of photon statistics and its mechanism.—To explore the nonclassical features of the system, we focus on the second-order correlation function $g^{(2)}(0)$ of the scattered signal field for the steady state, which can be calculated as $g^{(2)}(0) = \langle (\hat{P}^\dagger)^2 (\hat{P})^2 \rangle / \langle \hat{P}^\dagger \hat{P} \rangle^2$, where $\hat{P} = \chi a_1 + \mu \sigma_{12}$ is the total polarization operator. With the polarization operator, the intensity can be calculated as $I = \langle \hat{P}^\dagger \hat{P} \rangle$. We point that one can also use input-output formalism to calculate $g^{(2)}(0)$ and I , which is essentially equivalent to the above expressions [38]. In the following, we show that the quantum statistics can be controlled with the control field. As an example for proof-of-principle purposes, we consider a silver MNP (radius $r_m = 7$ nm) hereafter, whose dielectric constants are given by the Drude model $\varepsilon_m(\omega) = \varepsilon_\infty - \frac{\omega_p^2}{\omega(\omega+i\gamma)}$, with

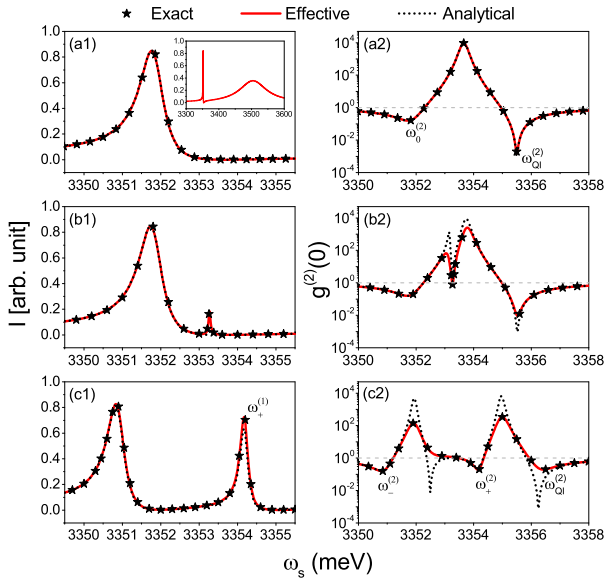


FIG. 2. (Color online) Scattered intensity (a1-c1) and second-order correlation (a2-c2) of the signal field versus the frequency ω_s for $\Omega_c = 0$ (a), $\Omega_c = 0.2$ meV (b), and $\Omega_c = 1.5$ meV (c). Results of exact multimode model (solid stars), effective model (red solid curves), and analytical results (black dotted curves) are shown, respectively. The inset of (a1) displays the intensity spectra for a broader frequency while the control field turns off. The control field is set to be resonant with the transition $|2\rangle \leftrightarrow |3\rangle$ ($\Delta_c = 0$).

the parameter being $\varepsilon_\infty = 4.6$, $\omega_p = 9.0$ eV, and $\gamma = 0.1$ eV [5]. Furthermore, the parameters of QE are set to be $\mu = 0.5$ enm, $\gamma_{21} = \gamma_{32} = 0.05$ meV, and $\omega_{21} - \omega_1 = -150$ meV. Placed in vacuum ($\varepsilon_b = 1$), the QE and MNP are separated by a distance $R = 12$ nm. We have considered a weak signal field with Rabi frequency $\Omega_s = 0.005$ meV.

Figure 2 shows the intensity I and photon correlation $g^{(2)}(0)$ of the signal field versus the frequency ω_s . Results of effective model (red solid line) and multimode model (solid stars) are shown respectively, from which We can see excellent agreement between these two models. When the control field turns off [Fig. 2(a)], this hybrid system is just the same with a two-level QE-MNP system, which has been investigated in Ref. [9]. In this case, the scattered intensity spectrum [Fig. 2(a1)] displays a single-peaked structure, whose peak is located near the resonance frequency of QE transition $|1\rangle \leftrightarrow |2\rangle$. In fact, this structure is a Fano line shape, which can be clearly seen from the inset of Fig. 2(a1) displaying the intensity spectrum for a broader frequency ω_s . This Fano structure originate from the coupling of between the continuum excitations of MNP and the discrete excitations of QE [39]. Particularly, as shown in Fig. 2(a2), the photon statistics can be controlled from bunching to antibunching just by tuning the frequency ω_s . Even so, in order to realize the active control of photon correlation we still need to know the effects of control field.

To this end, we plot the results when the control field

turns on in Fig. 2(b) ($\Omega_c = 0.2$ meV) and Fig. 2(c) ($\Omega_c = 1.5$ meV). For a relatively weak control field, we can see not only the different degree of the quantum correlation but also a new dip in $g^{(2)}(0)$ line shape [Fig. 2(b2)]. In addition, the intensity spectrum also shows a side peak centered at a frequency blue shifted from the main peak [Fig. 2(b1)]. Particularly, by further increasing the Rabi frequency of control field, the $g^{(2)}(0)$ shows more complex structures [Fig. 2(c2)]. There exist three frequency windows in which the scattered signal field shows antibunching statistics, which may provide versatile possibility to control the quantum statistics. Furthermore, the two peaks in intensity spectrum for this case have nearly the same amplitudes [Fig. 2(c1)]. This line shape can be understood from the conception of dressed state [40]. In other words, dressed by the control field, the QE level $|2\rangle$ splits into a pair of well separated levels, whose energies are given by

$$\omega_{\pm}^{(1)} = \omega_{21,\text{eff}} + \frac{1}{2} \left(\Delta_{c,\text{eff}} \pm \sqrt{\Delta_{c,\text{eff}}^2 + 4\Omega_c^2} \right). \quad (6)$$

In the case discussed above, the $\omega_-^{(1)}$ is near the frequency of Fano peak. Therefore, both the $\omega_-^{(1)}$ level and the Fano interference contribute to the low-energy peak, and thus this peak frequency is shifted compared with $\omega_-^{(1)}$ and the main peak for $\Omega_c = 0$. For the high-energy peak, its peak frequency is just located at $\omega_+^{(1)}$.

In order to gain deeper physical insights into the above results, we present an analytical treatment for the studied system. Under weak pumping conditions, the state of the hybrid system can be approximated as a pure state [11, 34, 41], whose evolution is governed by Schrödinger equation. After truncating the Hilbert space to two excitations, the state of the hybrid system in the rotating frame is

$$|\psi\rangle = |0, 1\rangle + C_{0,2}|0, 2\rangle + C_{0,3}|0, 3\rangle + C_{1,1}|1, 1\rangle + C_{1,2}|1, 2\rangle + C_{1,3}|1, 3\rangle + C_{2,1}|2, 1\rangle \quad (7)$$

where $|m, n\rangle$ denotes the plasmon Fock state $|m\rangle$ and QE level $|n\rangle$. The system dissipations can be included by considering a non-Hermitian Hamiltonian

$$H_{\text{eff}}^{\text{NH}} = H_{\text{eff}} - i\frac{\gamma_{21,\text{eff}}}{2}\sigma_{22} - i\frac{\gamma_{32}}{2}\sigma_{33} - i\frac{\kappa_1}{2}a_1^\dagger a_1. \quad (8)$$

Then the scattered intensity I is derived as

$$I = \mu^2 (|C_{0,2}|^2 + \xi^2 |C_{1,1}|^2 + 2\xi \text{Re}[C_{0,2}^* C_{1,1}]) = \mu^2 \Omega_s^2 \left| \frac{\tilde{\Delta}_1 + \xi^2 \left(\tilde{\Delta}_{s,\text{eff}} - \frac{\Omega_c^2}{\Delta_{s,\text{eff}}} \right) + 2\xi g_1}{\tilde{\Delta}_1 \left(\tilde{\Delta}_{s,\text{eff}} - \frac{\Omega_c^2}{\Delta_{s,\text{eff}}} \right) - g_1^2} \right|^2, \quad (9)$$

where $\tilde{\Delta}_1 = \Delta_1 - i\kappa_1/2$, $\tilde{\Delta}_{s,\text{eff}} = \Delta_{s,\text{eff}} - i\gamma_{21,\text{eff}}/2$, and $\tilde{\Delta}_{sc,\text{eff}} = \Delta_{s,\text{eff}} + \Delta_{c,\text{eff}} - i\gamma_{32}/2$. Moreover, the second-order correlation function can be determined by

$$g^{(2)}(0) = \frac{2\xi^2 (2|C_{1,2}|^2 + \xi^2 |C_{2,1}|^2 + 2\sqrt{2}\xi \text{Re}[C_{1,2}^* C_{2,1}])}{[|C_{0,2}|^2 + \xi^2 |C_{1,1}|^2 + 2\xi \text{Re}[C_{0,2}^* C_{1,1}]]^2}, \quad (10)$$

whose full expression is found to be

$$g^{(2)}(0) = \left| 1 - \frac{(\tilde{\Delta}_1 + \xi g_1)^2 \left[\tilde{\Delta}_1 \left(\tilde{\Delta}_{s,\text{eff}} - \frac{\Omega_c^2}{\Delta_{s,\text{eff}}} \right) - g_1^2 + (\tilde{\Delta}_1 + \xi g_1)^2 \left(1 + \frac{\Omega_c^2}{\Delta_{s,\text{eff}}(\tilde{\Delta}_1 + \Delta_{s,\text{eff}})} \right) \right]}{\left[\tilde{\Delta}_1 \left(\tilde{\Delta}_1 + \tilde{\Delta}_{s,\text{eff}} - \frac{\Omega_c^2}{\Delta_1 + \Delta_{s,\text{eff}}} \right) - g_1^2 \right] \left[\tilde{\Delta}_1 + 2\xi g_1 + \xi^2 \left(\tilde{\Delta}_{s,\text{eff}} - \frac{\Omega_c^2}{\Delta_{s,\text{eff}}} \right) \right]^2} \right|^2. \quad (11)$$

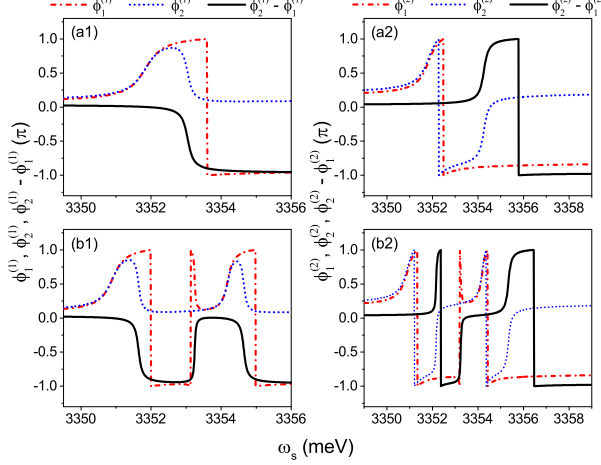


FIG. 3. (Color online) Phase parameters $\phi_1^{(1)}$, $\phi_2^{(1)}$, phase difference $\phi_2^{(1)} - \phi_1^{(1)}$ (a1, b1) and phase parameters $\phi_1^{(2)}$, $\phi_2^{(2)}$ and their difference $\phi_2^{(2)} - \phi_1^{(2)}$ as a function of ω_s for the case of $\Omega_c = 0$ (a1, a2) and $\Omega_c = 1.5$ meV (b1, b2).

The validity of these analytical results (dotted lines) is demonstrated in Fig. 2. When the control field is absent, excellent agreement can be found between analytical and numerical results. Though the agreements become poor with increasing Ω_c , the analytical results are still in qualitative agreement with the numerical solutions.

The analytical results illustrate the roles of the interference of probability amplitudes. Clear quantum interference signature are shown in Eqs. (9) and (10). For the intensity spectrum, the interference of $C_{0,2}$ and $C_{1,1}$, which are the probability amplitudes for one-quantum states $|0, 2\rangle$ and $|1, 1\rangle$, determines the line shape of intensity spectrum. While the interference between probability amplitudes of two-quantum states $|1, 2\rangle$ and $|2, 1\rangle$ determines the second-order correlation. In order to study the underlying quantum interference effects in depth, we introduce four phase parameters $(\phi_1^{(1)}, \phi_2^{(1)}, \phi_1^{(2)}, \phi_2^{(2)})$, which are the arguments of four complex probability amplitudes $(C_{0,2}, C_{1,1}, C_{1,2}, C_{2,1})$. It is obvious that the phase difference $\phi_2^{(1)} - \phi_1^{(1)}$ determines the interference properties of one-quantum amplitudes, while the phase difference $\phi_2^{(2)} - \phi_1^{(2)}$ gives the quantum interference effects on second-order correlation.

Figure 3 displays the phase parameters versus the frequency of signal field for the case of $\Omega_c = 0$ (a) and

$\Omega_c = 1.5$ meV (b). When the control field is absent, the interference properties are relatively simple. The first-order phase $\phi_1^{(1)}$ and $\phi_2^{(1)}$ interference constructively (destructively) below (above) the frequency $\omega_{21,\text{eff}}$. It is the transition from constructive to destructive interference that contributes to the one-peaked Fano structure in Fig. 2(a1). However, after exerting a strong control field, the QE level $|2\rangle$ splits into two dressed states, which leads to twice transitions from constructive to destructive interference [Fig. 3(b1)]. Hence the scattered spectrum for $\Omega_c = 1.5$ meV shows two peaks.

Next we focus on the quantum interference between two-quantum probability amplitudes. Without the control field, the amplitudes $C_{1,2}$ and $C_{2,1}$ interference destructively when $\omega_s > 3354$ meV. For an appropriate frequency, the third term in the numerator of Eq. (10) cancels the first two terms, which leads to the photon antibunching in Fig. 2(a2) around frequency $\omega_{\text{QI}}^{(2)}$. This particular interference effect is induced by the openness of plasmonic cavity. Although the amplitudes $C_{1,2}$ and $C_{2,1}$ interference constructively when $\omega_s < 3354$ meV, we can still observe photon antibunching effect around frequency $\omega_0^{(2)}$. We point out that this antibunching originates from the photon blockade effect. That is to say, the excitation to the lowest-energy state in the one-excitation manifold blocks subsequent excitation because the transitions to the two-excitation manifold are out of resonance [30]. By diagonalizing the Eq. (3) with the absence of driven fields, the $\omega_0^{(2)}$ is derived as

$$\omega_0^{(2)} = \omega_1 + \frac{1}{2} \left[\omega_{21,\text{eff}} - \omega_1 - \sqrt{(\omega_{21,\text{eff}} - \omega_1)^2 + 4g_1^2} \right]. \quad (12)$$

For the case with strong control field, three antibunching regions can be found. According to the phase difference between $\phi_1^{(2)}$ and $\phi_2^{(2)}$, the antibunching around $\omega_{\text{QI}}^{(2)}$ in Fig. 2(c2) is also induced by the destructive quantum interference. In contrast, there are two antibunching regions (denoted as $\omega_{\pm}^{(2)}$) induced by photon blockade for this case. Using the dressed states energy in Eq. (6), the $\omega_{\pm}^{(2)}$ read

$$\omega_{\pm}^{(2)} = \omega_1 + \frac{1}{2} \left[\omega_{\pm}^{(1)} - \omega_1 - \sqrt{(\omega_{\pm}^{(1)} - \omega_1)^2 + 4g_1^2} \right]. \quad (13)$$

So far we have shown the possibility of the photon correlation modulations by control field and the underlying

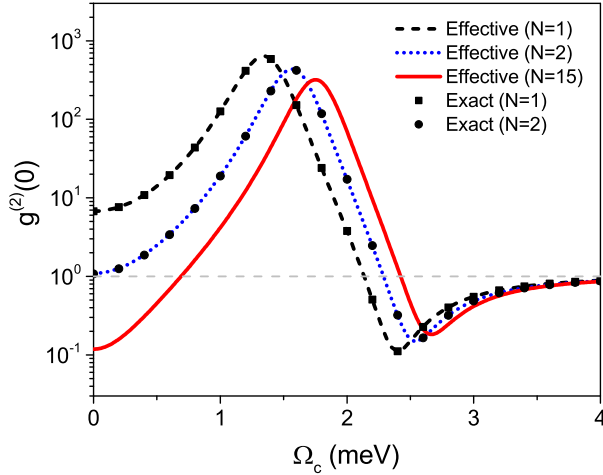


FIG. 4. (Color online) $g^{(2)}(0)$ correlation with respect to the Rabi frequency Ω_c of the control field calculated from effective model (red solid lines). To identify the role of higher modes, it is also shown that the results of considering only dipole mode ($N = 1$) and considering dipole and quadrupole modes ($N = 2$) calculated from effective model (dashed and dotted lines) and exact model (scatterers) respectively. The detuning Δ_s is fixed to $\Delta_s = -2$ meV.

quantum interference mechanism. In real applications, it is more desirable to realize the continuous modulation between bunching and antibunching. In the following, we show the all-optical modulation of photon correlation with the Rabi frequency Ω_c of control field in Fig. 4. When increasing the Rabi frequency Ω_c , the photon correlation of signal field makes a continuous transition from antibunching to bunching, and then to antibunching. The photon correlation tends to be disappear, that is, a field with random statistics, for strong control field ($\Omega_c > 4$ meV). Note that the coupling between QE and

MNP is not in strong coupling regime for the case studied here. However, the peculiar quantum interference effects enable us to control the photon correlations even in the bad cavity limit. Thus this results represent a nanoscaled scheme for all-optical control of photon statistics without the need of strong coupling condition. Compared the scheme in CQED, the scheme presented here is more compact and feasible. By the way, we point out that the impact of high-order modes of MNP is non-ignorable when the distance between QE and MNP is small. Neglecting the contribution of high-order modes may lead to a contrary prediction about the photon statistics [see the difference between solid and dashed curves in Fig. 4].

Conclusions.—To summarize, we have theoretically demonstrated the all-optical control of photon statistics with a hybrid QE-MNP system. We present three different ways for the studied system to uncover the non-classical correlation and underlying mechanisms. The analytical treatment reveals that the quantum interferences between two-quantum states' amplitudes are essential to the photon correlation modulation. Enriched by the dressed states, this quantum interference effects enable us to continuously regulate the photon correlation between bunching and antibunching. Compared with the CQED methods, this scheme is more compact and experimentally feasible as it works in the bad cavity limit. These results open an alternative possibility for the control of photon correlation, which may find its applications in quantum-optical devices.

ACKNOWLEDGMENTS

This work was supported by the Fundamental Research Funds for the Central Universities of China under Grant No. SWU116056.

[1] M. S. Tame, K. R. McEnery, S. K. Ozdemir, J. Lee, S. A. Maier, and M. S. Kim, “Quantum plasmonics,” *Nat. Phys.* **9**, 329 (2013).

[2] A. Trügler and U. Hohenester, “Strong coupling between a metallic nanoparticle and a single molecule,” *Phys. Rev. B* **77**, 115403 (2008).

[3] C. Van Vlack, P. T. Kristensen, and S. Hughes, “Spontaneous emission spectra and quantum light-matter interactions from a strongly coupled quantum dot metal-nanoparticle system,” *Phys. Rev. B* **85**, 075303 (2012).

[4] K. Slowik, R. Filter, J. Straubel, F. Lederer, and C. Rockstuhl, “Strong coupling of optical nanoantennas and atomic systems,” *Phys. Rev. B* **88**, 195414 (2013).

[5] A. Delga, J. Feist, J. Bravo-Abad, and F. J. Garcia-Vidal, “Quantum emitters near a metal nanoparticle: Strong coupling and quenching,” *Phys. Rev. Lett.* **112**, 253601 (2014).

[6] P. Peng, Y.-C. Liu, D. Xu, Q.-T. Cao, G. Lu, Q. Gong, and Y.-F. Xiao, “Enhancing coherent light-matter interactions through microcavity-engineered plasmonic resonances,” *Phys. Rev. Lett.* **119**, 233901 (2017).

[7] A. Ridolfo, O. DiStefano, N. Fina, R. Saija, and S. Savasta, “Quantum plasmonics with quantum dot-metal nanoparticle molecules: Influence of the fano effect on photon statistics,” *Phys. Rev. Lett.* **105**, 263601 (2010).

[8] R. Filter, K. Slowik, J. Straubel, F. Lederer, and C. Rockstuhl, “Nanoantennas for ultrabright single photon sources,” *Opt. Lett.* **39**, 1246 (2014).

[9] D. Zhao, Y. Gu, H. Chen, J. Ren, T. Zhang, and Q. Gong, “Quantum statistics control with a plasmonic nanocavity: Multimode-enhanced interferences,” *Phys. Rev. A* **92**, 033836 (2015).

[10] C.-J. Yang and J.-H. An, “Resonance fluorescence beyond the dipole approximation of a quantum dot in a plasmonic nanostructure,” *Phys. Rev. A* **93**, 053803 (2016).

[11] R. Sáez-Blázquez, J. Feist, A. I. Fernández-Domínguez,

and F. J. García-Vidal, "Enhancing photon correlations through plasmonic strong coupling," *Optica* **4**, 1363 (2017).

[12] D. Martín-Cano, H. R. Haakh, K. Murr, and M. Agio, "Large suppression of quantum fluctuations of light from a single emitter by an optical nanostructure," *Phys. Rev. Lett.* **113**, 263605 (2014).

[13] H. R. Haakh and D. Martín-Cano, "Squeezed light from entangled nonidentical emitters via nanophotonic environments," *ACS Photonics* **2**, 1686 (2015).

[14] C. Lee, M. Tame, C. Noh, J. Lim, S. A. Maier, J. Lee, and D. G. Angelakis, "Robust-to-loss entanglement generation using a quantum plasmonic nanoparticle array," *New J. Phys.* **15**, 083017 (2013).

[15] J. Hou, K. Słowiak, F. Lederer, and C. Rockstuhl, "Dissipation-driven entanglement between qubits mediated by plasmonic nanoantennas," *Phys. Rev. B* **89**, 235413 (2014).

[16] M. Otten, R. A. Shah, N. F. Scherer, M. Min, M. Pelton, and S. K. Gray, "Entanglement of two, three, or four plasmonically coupled quantum dots," *Phys. Rev. B* **92**, 125432 (2015).

[17] M. Otten, J. Larson, M. Min, S. M. Wild, M. Pelton, and S. K. Gray, "Origins and optimization of entanglement in plasmonically coupled quantum dots," *Phys. Rev. A* **94**, 022312 (2016).

[18] J. Hakami and M. S. Zubairy, "Nanoshell-mediated robust entanglement between coupled quantum dots," *Phys. Rev. A* **93**, 022320 (2016).

[19] J. Straubel, R. Sarniak, C. Rockstuhl, and K. Słowiak, "Entangled light from bimodal optical nanoantennas," *Phys. Rev. B* **95**, 085421 (2017).

[20] F. Zhang, D. Zhao, Y. Gu, H. Chen, X. Hu, and Q. Gong, "Detuning-determined qubit-qubit entanglement mediated by plasmons: An effective model for dissipative systems," *J. Appl. Phys.* **121**, 203105 (2017).

[21] T. Hartsfield, W.-S. Chang, S.-C. Yang, T. Ma, J. Shi, L. Sun, G. Shvets, S. Link, and X. Li, "Single quantum dot controls a plasmonic cavity scattering and anisotropy," *PNAS* **112**, 12288 (2015).

[22] S.-J. Ding, X. Li, F. Nan, Y.-T. Zhong, L. Zhou, X. Xiao, Q.-Q. Wang, and Z. Zhang, "Strongly asymmetric spectroscopy in plasmon-exciton hybrid systems due to interference-induced energy repartitioning," *Phys. Rev. Lett.* **119**, 177401 (2017).

[23] Y. Zhang, Q.-S. Meng, L. Zhang, Y. Luo, Y.-J. Yu, B. Yang, Y. Zhang, R. Esteban, J. Aizpurua, Y. Luo, J.-L. Yang, Z.-C. Dong, and J. G. Hou, "Sub-nanometre control of the coherent interaction between a single molecule and a plasmonic nanocavity," *Nat. Commun.* **8**, 15225 (2017).

[24] R. Chikkaraddy, B. de Nijs, F. Benz, S. J. Barrow, O. A. Scherman, E. Rosta, A. Demetriadou, P. Fox, O. Hess, and J. J. Baumberg, "Single-molecule strong coupling at room temperature in plasmonic nanocavities," *Nature (London)* **535**, 127 (2016).

[25] R. Liu, Z.-K. Zhou, Y.-C. Yu, T. Zhang, H. Wang, G. Liu, Y. Wei, H. Chen, and X.-H. Wang, "Strong light-matter interactions in single open plasmonic nanocavities at the quantum optics limit," *Phys. Rev. Lett.* **118**, 237401 (2017).

[26] M. O. Scully and M. S. Zubairy, *Quantum Optics* (Cambridge University Press, Cambridge, 1997).

[27] A. Reiserer and G. Rempe, "Cavity-based quantum networks with single atoms and optical photons," *Rev. Mod. Phys.* **87**, 1379 (2015).

[28] M. Kira, S. W. Koch, R. P. Smith, A. E. Hunter, and S. T. Cundiff, "Quantum spectroscopy with schrödinger-cat states," *Nat. Phys.* **7**, 799 (2011).

[29] A. Imamoğlu, H. Schmidt, G. Woods, and M. Deutsch, "Strongly interacting photons in a nonlinear cavity," *Phys. Rev. Lett.* **79**, 1467 (1997).

[30] K. M. Birnbaum, A. Boca, R. Miller, A. D. Boozer, T. E. Northup, and H. J. Kimble, "Photon blockade in an optical cavity with one trapped atom," *Nature (London)* **436**, 87 (2005).

[31] S. Rebić, A. S. Parkins, and S. M. Tan, "Photon statistics of a single-atom intracavity system involving electromagnetically induced transparency," *Phys. Rev. A* **65**, 063804 (2002).

[32] J. A. Souza, E. Figueroa, H. Chibani, C. J. Villas-Boas, and G. Rempe, "Coherent control of quantum fluctuations using cavity electromagnetically induced transparency," *Phys. Rev. Lett.* **111**, 113602 (2013).

[33] T. C. H. Liew and V. Savona, "Single photons from coupled quantum modes," *Phys. Rev. Lett.* **104**, 183601 (2010).

[34] M. Bamba, A. Imamoğlu, I. Carusotto, and C. Ciuti, "Origin of strong photon antibunching in weakly nonlinear photonic molecules," *Phys. Rev. A* **83**, 021802 (2011).

[35] C. F. Bohren and D. R. Huffman, *Absorption and Scattering of Light by Small Particles* (Wiley, New York, 1983).

[36] J. R. Johansson, P. D. Nation, and F. Nori, "Qutip: An open-source python framework for the dynamics of open quantum systems," *Comp. Phys. Comm.* **183**, 1760 (2012).

[37] J. R. Johansson, P. D. Nation, and F. Nori, "Qutip 2: A python framework for the dynamics of open quantum systems," *Comp. Phys. Comm.* **184**, 1234 (2013).

[38] E. Waks and D. Sridharan, "Cavity qed treatment of interactions between a metal nanoparticle and a dipole emitter," *Phys. Rev. A* **82**, 043845 (2010).

[39] W. Zhang, A. O. Govorov, and G. W. Bryant, "Semiconductor-metal nanoparticle molecules: Hybrid excitons and the nonlinear fano effect," *Phys. Rev. Lett.* **97**, 146804 (2006).

[40] C. Cohen-Tannoudji and S. Reynaud, "Dressed-atom description of resonance fluorescence and absorption spectra of a multi-level atom in an intense laser beam," *J. Phys. B: Atom. Molec. Phys.* **10**, 345 (1977).

[41] H. J. Carmichael, R. J. Brecha, and P. R. Rice, "Quantum interference and collapse of the wavefunction in cavity qed," *Opt. Commun.* **82**, 73 (1991).